Available online at www.sciencedirect.com
ScienceDirect
Trans. Nonferrous Met. Soc. China 34(2024) 1721−1733
Transactions of Nonferrous Metals Society of China
www.tnmsc.cn

Clarification of two-parameter models for correlating grain size to phase diagram variables in hypoeutectic alloys

Da-shan SUI[1], Qing-you HAN[2,3]

1. Institute of Forming Technology & Equipment, School of Materials Science and Engineering, Shanghai Jiao Tong University, Shanghai 200030, China;
2. School of Mechanical Engineering, Southeast University, Nanjing 211189, China;
3. School of Engineering Technology, Purdue University, West Lafayette, IN 47906, USA

Received 22 November 2022; accepted 16 May 2023

Abstract: Simple two-parameter models were proposed for correlating grain size to process conditions and phase diagram variables. However, these models have not been fully examined using data obtained from well controlled experiments. This work intended to clarify these models with selected experimental data obtained in dilute hypoeutectic alloys. Criteria for data selected were proposed. The selected experimental data were fitted by these models to examine curve fitting quality and the applicability. Models that fit experimental data better were identified. Mechanisms by which grain size is reduced under the influence of a solute element were examined based on the data analysis. Results suggest that there is a clear dependence of grain size on the solidification interval of an alloy, which can be expressed as the P variable. Such a clear dependence of grain size on solidification interval indicates that mechanisms that are associated with dendrite fragmentation are the dominant operating mechanisms governing grain refinement by solute element in ingots and castings where convection in the molten alloy exists during its mold filling and solidification.

Key words: solidification microstructure; grain refinement; solute element; mathematical model; phase diagram variables; grain size; hydroeutectic alloy

1 Introduction

Grain refining, i.e. reducing grain size, is beneficial to maximizing ingot casting rates [1], increasing resistance of an alloy to hot tearing [2,3], altering fluidity of an alloy during casting [4], and decreasing porosity formation in castings [5].

It is well known that two factors make major contributions to the refinement of the dendritic grains of as-cast metals and alloys: (1) suitable insoluble nucleant particles in the melt that nucleate dendritic grains [6], and (2) solutes that redistribute near the solid−liquid interface to alter the growth conditions of dendrites [7,8]. There is an interplay between these two factors. Nucleation has to occur at certain undercooling below the liquidus which is a function of solute content of the alloy. Solute-induced undercooling is essential to the growth, fragmentation, and survival of a grain. As a result, nucleant particles are capable of producing much smaller grains in an alloy containing solutes than those in a pure metal [9,10].

Simple two-parameter models have been proposed to correlate grain size d, with phase diagram variables under given casting conditions [11,12]. A widely used two-parameter model is in the form of [8]

$$d=a+b/Q \quad (1)$$

where a and b are two parameters which are

Corresponding author: Qing-you HAN, E-mail: hanq@purdue.edu; Da-shan SUI, Tel: +86-13916423049, E-mail: dasui@sjtu.edu.cn
DOI: 10.1016/S1003-6326(24)66502-7

affected by factors including the addition of grain refiners and the cooling conditions of the solidifying alloy [13], and Q is defined as [7]

$$Q=mC_0(k-1) \tag{2}$$

where C_0 is the bulk concentration of a binary alloy, m is the liquidus slope at C_0, k is the equilibrium partition coefficient, and Q is a phase diagram variable as it consists of phase diagram data, C_0, m and k. Q is also termed as growth restriction parameter [14,15] following an assumption made by MAXWELL and HELLAWELL [7] that the growth rate of a dendrite decreases with increasing Q. Many investigations were performed to establish the influence of casting conditions on a and b in Eq. (1). The model is probably supported by experiments performed in a thin slice of specimen solidified horizontally where convection in the melt is suppressed [16]. Main results are summarized in Ref. [17].

There are a few issues with Eq. (1).

First, the validity of Eq. (1) is not supported by experiments when C_0 and the resultant Q approach zero because the grain size has not been found to approach infinity. EASTON and STJOHN [8] reported that super-high-purity aluminum (99.995%) had similar grain size to 99.97% pure aluminum metal. Using high-purity aluminum metal directly taken from a smelter, HAN et al [18] measured grain size formed in the metal poured into a small copper mold and found that the grain size was about 1.6 mm. The grain size was reduced to about 400 μm by adding 0.5% Al−Ti−B master alloy into aluminum. Further addition of mater alloy from 0.5% to 1.5% into the melt did not result in further grain refinement. HAN et al [18] also demonstrated that the grain size was reduced from about 1.6 to 400 μm by injecting high-intensity ultrasonic vibration into the melt during its solidification. It could be argued that the addition of grain refiners would inevitably introduce solute titanium into the melt so that C_0 and the resultant Q would not be zero. However, the injection of ultrasonic vibration introduced no solutes into the melt so it had no effect on Q. Still, grain size was small regardless of Q approaching zero, indicating that Eq. (1) is not satisfactory in defining grain size when Q approaches zero.

Second, Eq. (1) implies that d approaches a when Q approaches infinity. However, such a relationship is not supported by the experimental results. The monotonic decreasing relationship between d and $1/Q$ at $C_0<C_{SL}$ breaks down when $C_0>C_{SL}$, where C_{SL} is the solubility limit of the solute in the primary dendritic phase [11,12]. ABDEL-REIHIM et al [19] found, in Pb−Sb alloy, that the grain size decreased with increasing C_0, reached a minimum at C_{SL}, and increased with a further increase in C_0, exhibiting a "U" shaped relationship. Such "U" shaped relationship was also found in Al−Si alloy [15] and Al−Cu alloy [20,21]. The issue with the "U" shaped curve can be resolved by using modified phase diagram variables or by plotting d vs ΔT, where ΔT is the solidification interval of an alloy at C_0 [11,12,20]. Still, the slopes of the curve at both sides of C_{SL} are different [11,12].

Third, the curve fitting quality of d vs $1/Q$ is not as good as that of d vs $1/P$ defined as [20,22,23]

$$P=\frac{mC_0(k-1)}{k} \tag{3}$$

Researchers who performed the controlled experiments on determining the relationship between grain size and phase diagram variables plotted their measured grain size against P [20,22,23]. The dependence of d on Q or P is associated with the dominant operative mechanisms of grain refining by a solute. The dominant mechanisms are still not fully understood and are still the focus of continued research [17].

To resolve the issues associated with Eq. (1), HAN [11,12] proposed the following two simple models:

$$d=a\exp(-bX) \tag{4}$$

$$d=\frac{1}{a+bX} \tag{5}$$

where X is Q, P, or ΔT, and ΔT equals P when $C_0<C_{SL}$. In Eqs. (4) and (5), d is a function of a at $X=0$. X equals ΔT or a modified P to resolve the issues with the "U" shaped curve and the curve linearity when $C_{SL}<C_0$. These models were newly proposed and have not yet been fully analyzed. Initial evaluation of these models with experimental data was performed but the data were not entirely from hypoeutectic alloys. Data cleaning is required.

To clarify the dominant mechanisms associated with the effects of a solute, the dependence of d on Q or P has to be critically

evaluated with experimental data from well-controlled experiments.

The purpose of the present study was to analyze the unique properties of the newly proposed models and to examine the influence of various phase diagram variables on grain size. Criteria for the selection of experimental data for model evaluated were proposed. Experimental data from literature [20,22,23] were filtered using the proposed criteria. Data analysis was performed using carefully selected data in dilute hypoeutectic alloys. Results from data analysis were then used for examining the dominant operative mechanisms of grain refining by solutes in alloys.

2 Methods

2.1 Data selection criteria

Experimental data on the influence of solute on grain size were taken from selected literature. Supplementary materials (SM) provides data used in this work. These data were selected from original data in Refs. [20,22,23] by using our criteria for data selection.

The criteria for data selection included: (1) dilute hypoeutectic alloys ($C_0<C_{SL}$), (2) fixed pouring temperature at a given superheat so that the cooling rates of the ingots with various solute contents were identical, (3) identical population density of potent nucleant particles, (4) the alloy composition being the content of solute in the melt at the moment when dendrites start to form (this requirement would eliminate peritectic alloys where solute elements would form solid compounds prior to dendritic solidification since elements in the solid compounds cannot affect grain size as solutes), and (5) involving pouring a melt into a mold cavity so that a certain amount of convection existed in the melt prior to its solidification (this is a basic requirement for making a casting).

Limited experimental results are available based on the selection criteria described above. The selected data provided by SPITTLE and SADLI [23] were chosen. Their work was performed at a fixed pouring temperature. Superheat could be considered constant because only dilute alloys were cast. Their experimental data on peritectic Al−Cr and Al−Zr alloys were not used due to Criterion 4. Their data on Al−Fe, Al−Mn and Al−Sn alloys were removed due to Criterion 1.

Data by XU et al [20] in the composition range of $C_0<C_{SL}$ were also selected. Their work was carried out using metals of high purity. Ingots were made under conditions where the melt was poured at a given superheat while the temperature difference between the pouring temperature and the mold temperature was fixed. Under such conditions, the cooling rates in ingots of various compositions were identical.

Data by TARSHIS et al [22] in the composition range of $C_0<C_{SL}$ were used. Their work was performed under extremely well controlled conditions where potent nucleant particles were totally removed by repeated remelting to achieve supercooling at which nucleation of the dendritic phase occurred spontaneously. Their data on the Ni−W system were removed based on Criteria 1 and 4. As a result, their data on hypoeutectic alloys $C_0<C_{SL}$ of were used in this study.

2.2 Determining model parameters from measured grain size

To determine the model parameters a and b from measured grain size data, Eqs. (4) and (5) have to be transformed into linear relationships in the forms of

$$\ln d=\ln a-bX \tag{6}$$

$$1/d=a+bX \tag{7}$$

These linear relationships offer a simple way to test the applicability of these models to the measured grain size data and to calculate parameters, a and b, by linear regression.

2.3 Determining model parameters from measured relative grain size

Data by TARSHIS et al [22] were reported as relative grain size in an alloy to its pure base metal, making the data impossible to analyze using Eq. (1). However, their data can be processed using Eqs. (4) and (5). These equations have to be transformed so that the measured relative grain size could be used for determining model parameters.

Let d_0 be the grain size of the pure metal, i.e.,

$$d=d_0\big|_{X=0} \tag{8}$$

and b_0 be the gradient of d at X=0 defined by

$$b_0=\left.\frac{\mathrm{d}d}{\mathrm{d}X}\right|_{X=0} \tag{9}$$

a and b in Eqs. (4) and (5) can be obtained as

functions of d_0 and b_0 by using Eqs. (8) and (9), so that Eqs. (4) and (5) can be rewritten as

$$d=d_0\exp(\frac{b_0}{d_0}X) \tag{10}$$

$$d=\frac{d_0}{1-(b_0/d_0)X} \tag{11}$$

Rearranging Eqs. (10) and (11) yields

$$\frac{d}{d_0}=\exp\left(\frac{b_0}{d_0}X\right) \tag{12}$$

$$\frac{d}{d_0}=\frac{1}{1-(b_0/d_0)X} \tag{13}$$

Equations (12) and (13) become dimensionless. The left side of these equations, d/d_0, is the relative grain size in respect to the grain size of pure metal. It is also the grain size normalized to that of the pure metal. Xb_0/d_0 is also dimensionless where b_0/d_0 is the relative gradient of grain size with respect to a phase diagram variable X at C_0=0 or X=0. b_0/d_0 can also be used as a measure of the effectiveness of grain refinement of a pure metal by a phase diagram variable in given casting conditions.

2.4 Calculating phase diagram variables

Liquidus slope, m, and partition coefficient, k, of selected alloys are given in Table 1.

Table 1 Phase diagram data of selected binary alloys [12]

Alloy	k	m/(°C·wt.%$^{-1}$)
Al−Cu	0.17	−3.43
Al−Mg	0.51	−6.20
Al−Si	0.11	−6.60
Al−Zn	0.43	−1.65

Q and P were calculated using Eqs. (2) and (3) and phase diagram data in Table 1 for the selected alloy systems listed in Table S1 of Supplementary Materials (SM). The solidification interval, ΔT, of each selected alloy was calculated using the latest aluminum database and PandaTM Software by CompuTherm. The calculated Q, P and ΔT are also given in SM.

3 Results

Table 2 summaries the curve fitting results using the two-parameter models and selected data from literature given in SM. The data selected from literature contain X=0, where X in the two-parameter models represents Q, P, or ΔT (all these three phase diagram variables are listed under each model) in Table 2. a, b and R^2 in Table 2 are obtained by linear regression using Eqs. (1), (6), or

Table 2 Curve fitting results

Alloy	Parameter	$d=a\exp(-dX)$			$d=1/(a+bX)$			$d=a+b/X$		
		ΔT	Q	P	ΔT	Q	P	ΔT	Q	P
Wrought alloys (No grain refiners) [23]	a	3.1×10^{3}	3.09×10^{3}	2.81×10^{3}	1.0×10^{-4}	9.0×10^{-5}	2.0×10^{-4}	(1.23×10^{3})	(1.24×10^{3})	(1.38×10^{3})
	b	2.1×10^{-2}	1.15×10^{-2}	1.61×10^{-2}	2.0×10^{-5}	1.0×10^{-4}	2.0×10^{-5}	(9.21×10^{3})	(1.76×10^{3})	(4.82×10^{3})
	R^2	0.72	0.65	0.70	0.60	0.58	0.64	0.0(0.60)	0.0(0.50)	0.0(0.53)
Wrought alloys (with grain refiners) [23]	a	3.29×10^{2}	3.02×10^{2}	2.84×10^{2}	3.4×10^{-3}	4.0×10^{-4}	1.0×10^{-3}	(1.03×10^{2})	(1.20×10^{2})	(1.20×10^{2})
	b	1.6×10^{-2}	7.4×10^{-2}	1.1×10^{-2}	7.0×10^{-5}	3.0×10^{-4}	5.0×10^{-5}	(1.51×10^{3})	(2.32×10^{2})	(8.74×10^{2})
	R^2	0.54	0.39	0.43	0.68	0.41	0.59	0.0(0.86)	0.0(0.63)	0.0(0.81)
Casting alloys [20]	a	2.13×10^{3}	1.67×10^{3}	1.91×10^{3}	3.0×10^{-4}	6.0×10^{-4}	4.0×10^{-4}	(1.16×10^{2})	(4.05×10^{2})	(6.26×10^{2})
	b	1.8×10^{-2}	4.8×10^{-2}	1.5×10^{-2}	2.0×10^{-5}	5.0×10^{-5}	2.0×10^{-5}	(9.36×10^{3})	(3.75×10^{3})	(7.61×10^{3})
	R^2	0.91	0.62	0.88	0.90	0.55	0.93	0.0(0.74)	0.0(0.93)	0.0(0.81)
Ultra-clean Ni alloys [22]	a			0.58			1.80			
	$b(=-b_0/d_0)$			0.05			0.22			
	R^2			0.75			0.92			
Ultra-clean Al alloys [22]	a			0.62			1.95			
	$b(=-b_0/d_0)$			0.03			0.11			
	R^2			0.68			0.87			

(7), where R^2 is a statistical measure that represents the proportion of the variance for d by X in a regression model. The curve fitting quality increases with increasing R^2. Data in brackets listed under Eq. (1) in Table 2 were obtained when the experimental data at X=0 were removed because the equation is not valid at X=0. The R^2 values listed under Eq. (1) in Table 2 are zero because d at X=0 using Eq. (1) is infinity, indicating that Eq. (1) should not be used for describing d vs X in dilute alloys, especially C_0 approaches zero. One conclusion that can be made from the R^2 in Table 2 is that the values are significantly higher than those reported in Refs. [11,12] because the data selection criteria were used for data filtering.

Different from Eq. (1), both Eqs. (4) and (5) can be used for curve fitting with experimental data at X=0. The R^2 values of Eqs. (4) and (5) containing X=0 are much higher than that of Eq. (1) which has R^2=0. Even with X=0 data removed using Eq. (1), the R^2 values of Eqs. (4) and (5) containing X=0 are still comparable to, if not better than, that of Eq. (1) that excludes X approaching zero, indicating that Eqs. (4) and (5) are better than Eq. (1) in describing the dependence of grain size on phase diagram variables.

Theoretically, $P=\Delta T$ when $0\leq C_0\leq C_{SL}$ [11]. As a result, the curves of d vs P and d vs ΔT should overlap so that the data of a, b, and R^2 listed under P and ΔT in Table 2 should be the same. This is obviously not the case. Most likely, it is because the liquidus slope and partition coefficient are not constant when the bulk composition, C_0, is varied. P in Table 2 is calculated using Eq. (3) and constants listed in Table 1, implying that the liquidus and solidus are straight lines. ΔT in Table 2 is calculated at a given C_0 using thermodynamic database and software regardless of the shapes of the liquidus and solidus. The R^2 values associated with the curves of d vs ΔT are slightly higher than those of d vs P, probably indicating that ΔT is more accurate than P.

Comparing the R^2 values for Eqs. (4) and (5) given in Table 2, one can make a conclusion that the curve fitting quality of d vs ΔT is better than that of d vs P, and d vs P is better than d vs Q. For a fair comparison of curve fitting quality, d vs P should be compared with d vs Q, since both phase diagram variables are calculated using constants k and m.

3.1 Wrought alloys

Figure 1 illustrates the curve fitting quality of Eq. (1) and experimental data reported by SPITTLE and SADLI [23]. The solid markers are the experimental data and the curves are calculated using Eq. (1) with the a and b values (listed under Q in Table 2) obtained in linear regression shown in Fig. 1(b).

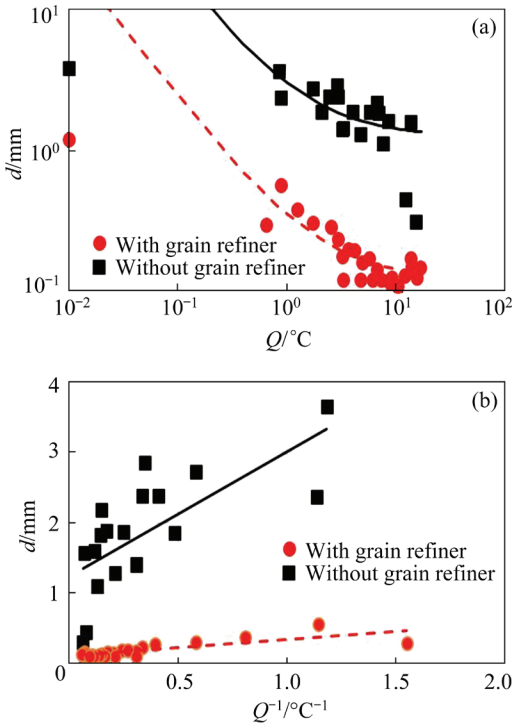

Fig. 1 Curve fitting results of Eq. (1) to experimental data in aluminum wrought alloys [23]: (a) $Q\geq$0.01 °C; (b) Q>0.5 °C

Figure 1(a) shows that, when Q<0.5 °C, the curve deviates significantly from experimental data. The predicted d using Eq. (1) approaches infinity as Q approaches zero. Such a trend of the predicted curve is associated with an inherent issue of Eq. (1) and is the reason that Eq. (1) is inappropriate in describing the dependence of grain size on phase diagram variables in dilute alloys when Q is small.

Figure 1(b) depicts the curve fitting quality for alloys when Q>0.5 °C. Equation (1) fits with experimental data reasonably well, except for alloys of high Q values. The curve fitting quality for the grain-refined alloys is better than that for the alloys that are not grain refined.

A significant improvement in the quality of curve fitting is achieved when using Eq. (1) to fit data listed in SM as compared with that from the

entire dataset reported in Ref. [11]. The R^2 values are 0.5 and 0.63 for alloys without adding grain refiners and with grain refiners, respectively. These values are significantly higher than those reported in Refs. [11,12] where these values are 0.079 and 0.417, respectively. The difference in the quality of curve fitting using selected data and the original data can also be seen clearly by comparing Fig. 1(b) of this work and Fig. 8 of Ref. [11]. Obviously, the original data contain alloys with $C_0 \geq C_{SL}$ or having peritectic reactions. The former causes the formation of the "U" shaped curves and the latter results in elements being consumed as intermetallic particles which affect the nucleation, but not the growth, of the aluminum dendritic phase. Data cleaning using the criteria described in Section 2.1 is important in establishing the relationship between grain size and phase diagram variables that truly reflect the effect of solute on grain size in the composition range of $C_0 \leq C_{SL}$.

Figure 2 illustrates the results using Eq. (4) to fit the experimental data in wrought aluminum alloys [23]. Generally speaking, Eq. (4) fits the experimental data better than Eq. (1) by comparing Figs. (1) and (2), especially for alloys without grain refiner. Note that data associated with Q<0.5 have been removed from Fig. 1(b) but retained in Fig. 2.

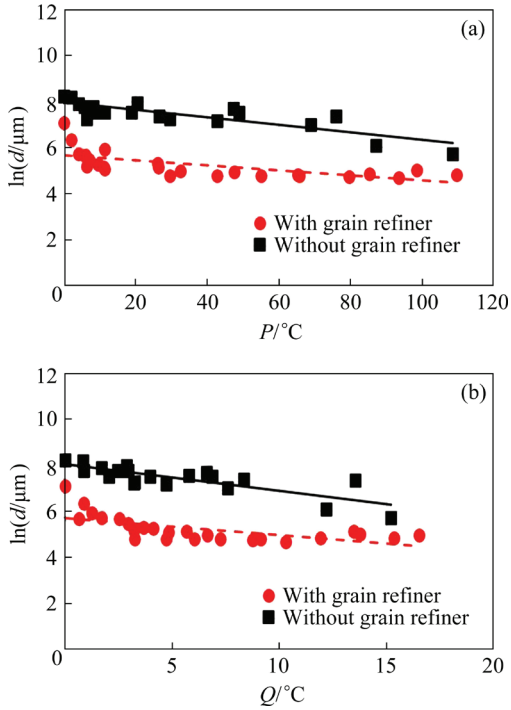

Fig. 2 Curve fitting results of Eq. (4) to experimental data in aluminum wrought alloys [23]: (a) d vs P; (b) d vs Q

Comparing Figs. 2(a) and (b), one can see that the curve fitting quality of the d vs P curves is slightly better than that of d vs Q. This is because the R^2 associated with the d vs P curves is slightly greater than that associated with the d vs Q curves.

Figure 3 depicts the curve fitting quality of Eq. (5) to experimental data obtained in wrought aluminum alloys [23]. Once again, the R^2 associated with the d vs P curves is slightly greater than that associated with the d vs Q curves. The curve fitting qualities of the d vs P curves shown in Fig. 3(a) are better than those of the d vs Q curves shown in Fig. 3(b).

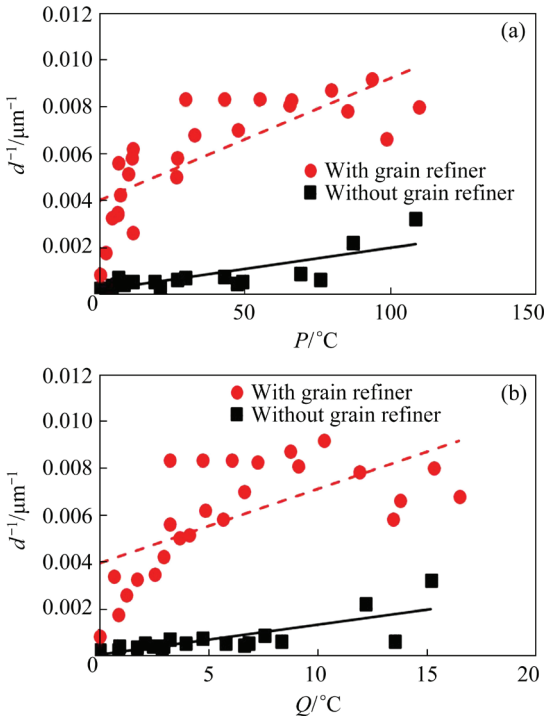

Fig. 3 Curve fitting results of Eq. (5) to experimental data in aluminum wrought alloys [23]: (a) d vs P; (b) d vs Q

3.2 Casting alloys

Figure 4 represents curve fitting results of casting alloys [20] using Eqs. (4) and (5), where the black color represents results associated with Eq. (4) and red color with Eq. (5). The solid markers and dash lines illustrate data associated with d vs Q and the open markers and solid lines with d vs P. Results shown in Fig. 4 and Table 2 suggest that the curve fitting quality of d vs P is much better than that of d vs Q. Note that experiments on these casting alloys were controlled extremely well that the superheat and the temperature difference

between the pouring temperature and the mold temperature were kept constant.

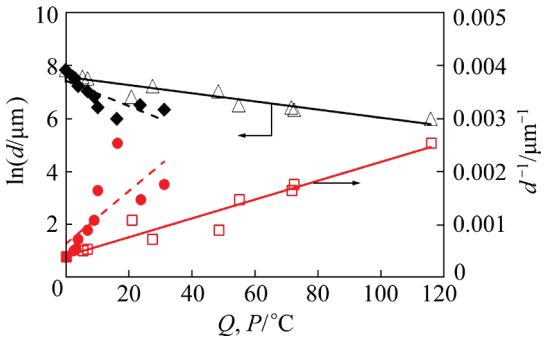

Fig. 4 Curve fitting results using Eq. (4) (black color) and Eq. (5) (red color) to fit experimental data in aluminum casting alloys (◆, ● and dash lines are associated with Q; □, Δ and solid lines are associated with P)

3.3 Ultra-clean alloys

One benefit of using Eqs. (4) and (5) is that the relative grain size in respect to the grain size of a pure base metal can be described in the forms of Eqs. (12) and (13). Such a relative grain size cannot be handled using Eq. (1) because d is infinity at Q=0.

Figure 5 presents the relationship between relative grain size and P in catalytically clean alloys, where heterogeneous nucleus are inactive due to repeatedly remelting of an alloy before pouring. It can be seen clearly from Fig. 5 and data listed in Table 2 that the curve fitting quality and linearity of Eqs. (4) and (5) are reasonably good. The curves can be forced to pass d=d_0 at P=0. However, the R^2 values of the curve associated with d=d_0 at P=0 are smaller, indicating the existence of measurement errors on grain size, which are not given in the literature.

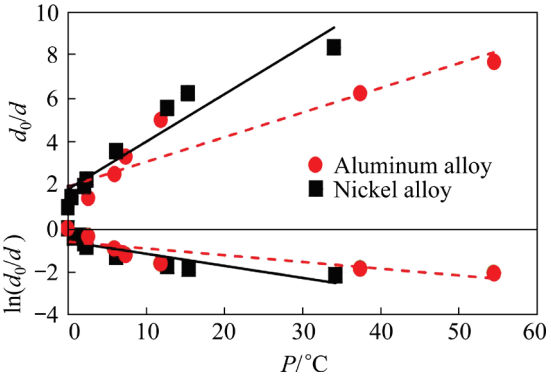

Fig. 5 Curve fitting results using Eqs. (4) and (5) to fit experimental data

4 Discussion

4.1 Model comparison

Results shown above suggest clearly that Eqs. (4) and (5) are capable of describing the effects of solute on grain refining in dilute alloys including pure base metals, where C_0 or the resultant X approaches zero. The widely used two-parameter equation, i.e. Eq. (1), is not suitable for such metals and alloys because the equation has a mathematical singularity at X=0. As a result, Eq. (1) is not well defined near X=0 so the equation is lack of analyticity for dilute alloys when C_0 approaches zero.

In the composition range of $0\leq C_0\leq C_{SL}$, Eqs. (4) and (5) were used. When $0<C_0\leq C_{SL}$, all three models, i.e. Eqs. (1), (4) and (5), describe the dependence of d vs X fairly well. d decreases monotonically with increasing X. Analysis results shown above indicate that the d vs ΔT curves fit with experimental data better than the d vs P curves and the d vs P curves are better than the d vs Q curves, especially if Eqs. (4) and (5) are used.

When $0<C_0\leq C_E$, where C_E is the eutectic composition of a hypoeutectic alloy, the d vs P or Q curves become "U" shaped while the d vs ΔT curves are still monotonic [11,12]. By removing data associated with $C_0>C_{SL}$ from Refs. [25−27], one could obtain R^2 much higher than that reported by HAN [11,12] who analyzed the same datasets previously, especially for the curves of the d vs P or Q. Such results suggest that Eqs. (1), (4) and (5) are good for describing d vs P or Q only in the region of $C_0\leq C_{SL}$. The "U" shaped relationships are described in Refs. [11,12]. To describe the dependence of grain size on a phase diagram variable over the entire composition range of a hypoeutectic alloy, i.e. $0\leq C_0\leq C_E$, Eqs. (4) and (5) with X=ΔT have to be used as reported by HAN [11,12].

The applicability of these two-parameters models with the best phase diagram variable has to be understood based on the physical meanings of phase diagram variables and mechanisms of grain refinement associated with each phase diagram variable.

4.2 Physical meaning of phase diagram variables

The physical meanings of P and Q were

discussed in literature extensively [21−23,25−27]. General consensus is that P is the constitutional supercooling parameter [20,22,23] and Q is the growth restriction parameter [8,14,15]. Such a consensus does not fully reflect the physical meanings of these two variables, which have to be understood from solute redistribution during solidification of an alloy.

Figure 6 illustrates the composition profiles (green curves) and corresponding liquidus temperature profiles (red curves) in the solid and liquid when the solid grows with a planar interface at a constant rate R, under a constant temperature gradient G, assuming the temperature distribution T_R, ahead of the freezing front is linear, and k and m are constant. The solid grows from the left side towards the right side of the sample shown in the middle of Fig. 6. The bulk composition of the sample is C_0 and $C_0 \leq C_{SL}$. A corner of a phase diagram of a eutectic containing alloy is shown on the right side of the composition profiles.

Analytical equations for the composition profiles were obtained by SMITH et al [24]. The composition of the first layer of solid forming from the liquid is kC_0, and its corresponding liquidus temperature is T_T and solidus temperature is T_L. T_L is also the liquidus of the alloy with a bulk concentration of C_0. Since the composition difference between this first layer of solid and the bulk liquid is $C_0(k-1)$, the corresponding temperature difference is $mC_0(k-1)$ which is Q. Thus, the liquidus temperature of the first layer of solid can be read from the phase diagram and is T_T, which is given by [28, 29]

$$T_T = T_L + mC_0(k-1) = T_L + Q \tag{14}$$

The solidification interval of this first layer of solid is $Q(=mC_0(k-1))$ as shown in Fig. 6.

It is important to note that T_T is higher than T_L by Q, indicating that the first layer of solid is constitutionally superheated with respect to the bulk liquid alloy by Q. This first layer of solid is usually the solid embryo and is non-dendritic. Because its liquidus, T_T, is higher than T_L, the growth of the solid embryo is restricted [7], so Q is termed as the growth restriction parameter.

Another important physical meaning of Q is related to T_T that is not only the liquidus temperature of the solid embryo but also the melting-to-dissolution transition temperature of the embryo when it is placed above the liquidus temperature of an alloy [28,29]. HAN and HELLAWELL [28] observed that the melting-to-dissolution temperature of a solid crystal was higher than the liquidus T_L of an alloy, and found that there are two rates associated with the disappearing of the solid crystal in the melt: the faster one was associated with melting and was

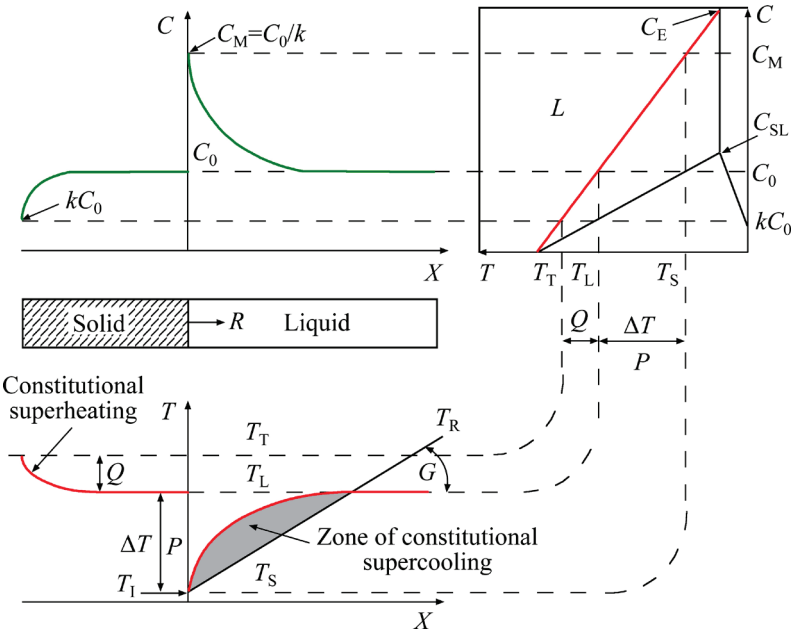

Fig. 6 Schematic illustration of composition and temperature profiles and meanings of P and Q when solid growing at constant rate under constant temperature gradient

controlled by heat transfer between the melt and the solid, and the slower one was associated with the dissolution of the solid and was controlled by the mass transfer between the melt and the solid. The transition temperature between melting and dissolution was defined as T_T. Solid embryos would be survival in a melt much longer if the melt temperature is within the temperature range of Q above T_L of the alloy with bulk concentration C_0. VIAN et al [29] found that grain size was much smaller when the melt was poured within Q above the liquidus temperature of the alloy. The survival time of embryos or dendritic fragments strongly affects the final grain size in solidified ingots.

As the solid shown in Fig. 6 continues to grow, the composition of the newly formed solid layer increases quickly, reaches C_0 where the growth enters steady-state growth conditions, and stays at C_0 until the solid front enters the end zone on the right side of the sample [24]. Under the steady-state conditions, the composition and temperature profiles in the liquid ahead of the growing solid are shown in Fig. 6. Solute is enriched ahead of the freezing front due to solute partitioning. The maximum composition, C_M, in the liquid occurs at the solid−liquid interface, where

$$C_M=C_0/k \tag{15}$$

and the corresponding liquidus temperature, T_I, at the solid−liquid interface is given by

$$T_I=T_L-mC_0(k-1)/k=T_L-P \tag{16}$$

Figure 6 illustrates that P is the temperature depression at the solid−liquid interface caused by solute segregation. HAN [12] proved analytically that when $C_0\leq C_{SL}$,

$$P=\Delta T \tag{17}$$

It is important to note that P is not the constitutional supercooling illustrated in Fig. 6 although it has been termed as the constitutional supercooling parameter.

When $C_E\geq C_0>C_{SL}$, Eq. (15) is not valid anymore because the peak concentration, C_M, would be limited by the eutectic composition, C_E, as shown in Fig. 6, meaning that eutectic phases would form when $C_M=C_E$. Since the eutectic front does not reject solute, C_M would always equal C_E and is smaller than C_0/k when $C_0>C_{SL}$. The use of Eq. (15) would greatly over estimate C_M and the resultant P as illustrated by XU et al [20]. In such a composition range, the composition difference, ΔC, between C_M and C_0 is

$$\Delta C=C_M-C_0=C_0\left(\frac{1}{C_0/C_E}-1\right) \tag{18}$$

Let

$$k^*=C_0/C_E \tag{19}$$

Substituting Eq. (19) into Eq. (18), one can write the interface temperature of the solid−liquid interface in alloys with $C_E\geq C_0>C_{SL}$ as

$$T_I=T_L-mC_0(k^*-1)/k^*=T_L-P^* \tag{20}$$

where P^* is given by

$$P^*=\frac{mC_0\,(k^*-1)}{k^*} \tag{21}$$

HAN [12] proved analytically that P^* equals ΔT and is the temperature depression at the solid−liquid interface [11,12] in alloys with $C_E\geq C_0>C_{SL}$.

The above analysis indicates that Q specifies the range of superheat (T_T-T_L) within which the solid embryos dissolve into the melt, and P or P^* equals ΔT and is the temperature depression at the solid−liquid interface under steady-state growth conditions. Because Q is related to T_T and $kC_0\leq C_{SL}$, Q defined by Eq. (1) can be used for the entire composition range of a hypoeutectic alloy, i.e., $0\leq C_0\leq C_E$. Because C_0/k has to be equal to or smaller than C_0, P has to be defined by Eq. (3) when $C_0\leq C_{SL}$ and by Eq. (21) when $C_E\geq C_0>C_{SL}$ to avoid being over-estimated. The overestimation of P in the composition range of $C_E\geq C_0>C_{SL}$ is coincident with the right side of the "U" shaped relationship between d and Q or P.

4.3 Nature of "U" shaped relationships between *d* and *Q* or *P*

Since the growth restriction factor described by Q is valid in the composition range of $0\leq C_0\leq C_E$, grain size should decrease monotonically with increasing Q over the entire composition range of a hypoeutectic alloy. This is certainly not the case as numerous works have demonstrated that d vs Q exhibits a "U" shaped relationship [11,12,15,19,20].

The "U" shaped relationship has also been found when plotting d against P in hypoeutectic alloys [11,12,20]. We found in this present work that the curve fitting qualities are improved comparing to that in Ref. [12] by removing data

with $C_0 \geq C_{SL}$ from the same datasets. Furthermore, HAN [11,12] found that the d vs ΔT curves are monotonous over $0 \leq C_0 \leq C_E$. The d vs P curves are also monotonous over $0 \leq C_0 \leq C_E$ if one uses $P=P^*$ when $C_E \geq C_0 > C_{SL}$. These findings strongly suggest that the formation of the "U" shaped relationship is closely related to the over-estimation of P when k and m are assumed to be constant in the composition range of $C_E \geq C_0 > C_{SL}$. It is evident that the mechanisms that are associated with P are the operating mechanisms governing the grain refinement of alloys when the melt is poured into a mold for making ingots and castings.

4.4 Mechanisms of grain refinement by solute element

Mechanisms that are associated with grain refining by a solute element have been well described. These mechanisms include constitutional supercooling, free chill crystal formation, dendrite arm remelting, grain separation from mold surface which is also related to dendrite arm remelting, and others such as crystal showering from the melt surface.

The constitutional supercooling mechanism has been widely used for explaining the d vs Q relationship in the past two decades. The basic idea is that solute enriched ahead of the freezing front causes the formation of constitutional supercooling zone in which new grains can be formed when the constitution supercooling is greater than a critical nucleation undercooling. As a result, grain formation is controlled by a wave of nucleation events proceeding the solidification front. In given cooling and nucleation conditions, grain size decreases with increasing Q because the growth rates of the solid embryos decrease with increasing Q, allowing more new grains to form nearby an existing grain. The mechanism is supported by experiments carried out in thin horizontal slice specimens solidified directionally where convection in the melt is suppressed [16]. However, as pointed out by CHALMERS [30], such a mechanism should only be used under conditions where convection is minimized. Experimental data used in this study were from cast ingots of substantial size involving the step of pouring a molten metal into casting molds. Convection in these ingots was significant. Thus, the constitutional supercooling mechanism should not be used in explaining grain refining by a solute element.

Mechanisms associated with the dendrite fragmentation and multiplication should be used for interpreting the relationship between grain size and phase diagram variables obtained in this study.

Considering a growing dendrite, its tip grows like an embryo with the compositions similar to the first layer of solid shown in Fig. 6. The roots of its secondary dendrite arms would have composition similar to that near the solid−liquid interface under steady-state conditions shown in Fig. 6, where the temperature depression at the solid−liquid interface is ΔT which equals P when $C_0 \leq C_{SL}$ or P^* when $C_0 > C_{SL}$. Such a temperature depression causes necking formation at the root of each secondary dendrite. The necks at the root of dendrite could be easily remelted or dissolved if local temperature fluctuation occurs. Coarsening due to Ostwald ripening could also cause the dissolution of a dendrite at its neck because the neck has a smaller radius than the neighboring part of the dendrite. The fragments that are separated from their mother dendrite could be brought to the bulk of the liquid by convection.

There is a large body of literature supporting the mechanisms of dendrite fragmentation and multiplication including vertical solidification of thin slice specimens [25,31], gravity casting processes such as direct-chill casting [26,32], forced mold filling processes such as die casting [27], and solidification under forced flow using external stirring [33] or external fields [34].

X-ray radiography revealed the dendrite fragmentation and the floating of fragments ahead of freezing front in vertically solidifying thin-slice alloys due to density difference between the solid dendrite and the melt [25,31]. In thin-slice transparent materials solidified horizontally, fragments were observed being carried out of the mushy zone by bubbles [35].

The direct-chill casting process is probably the most quiescent metal casting process, where the maximum flow speed in the sump is only a few millimeters per second [36]. Floating grains have been extensively reported and described [26,32]. Their size can be as large as a few hundred micrometers [32] and they can be found as anywhere in an ingot. As much as over 68% of the grains in the center of a direct-chill cast ingot comprising floating grains [37].

For other gravity casting processes including the processes where the data used in this study were obtained, the flow rate during the pouring of a hot melt is orders of magnitude greater than that during the direct-chill casting process. Consequently, fragmentation should be much severer. The circulation of fragments in the melt would practically eliminate the opportunity of nucleation of new grains. This is because the fragments are much larger than newly formed solid embryos. These small embryos, if they can be nucleated, would dissolve quickly when large solid fragments approach them due to Ostwald coarsening.

It is reasonable to argue that dendrite fragmentation and multiplication are the main operating mechanisms that govern grain refinement by solute in castings and ingots made by gravity casting processes. Since dendrite fragmentation is closely related to neck formation that is a direct result of temperature depression at the roots of dendrite, the influence of solute on grain refining should be evaluated by phase diagram variables of P or ΔT. This would account for the correlation between the "U" shaped relationship of d vs P because the over-estimate of P at $C_0>C_{SL}$, and the monotonic relationship between d vs ΔT over the entire composition range of a hypoeutectic alloy.

Still, Q is also important in affecting grain size. The growth rates of non-dendritic embryos are associated with Q, as well as the leading tip of a primary dendrite arm [7]. Grain size should decrease with decreasing growth rates associated with an increase in Q. Arguably, this growth restriction effect is also included in P because $P=Q/k$ when $C_0\leq C_{SL}$.

Another important aspect of Q affecting grain size is associated with temperature range (above the liquidus) within which dendrite fragments dissolve slowly into the melt rather than melt quickly in the melt. Fragments would survive for a certain amount of time depending on their size and local temperature [25]. Dissolution of a fragment would also accelerate dendrite multiplication if a large branch of primary dendrite is brought into the superheated liquid. It remains to be examined if the "Big Bang" phenomenon, i.e. the formation of small grains when the melt is poured with a small superheat above the liquidus of alloy, is associated with pouring a melt within a superheat of Q.

5 Conclusions

(1) When the bulk composition of an alloy approaches zero, two-parameter models that have singularity at $C_0=0$ must not be used to correlate the grain size to phase diagram variables for hypoeutectic alloys.

(2) In the composition range of $0<C_0\leq C_{SL}$, all three two-parameter models fit with experimental data reasonably well. However, the dependence of grain size on P or ΔT is better than on Q.

(3) Care must be taken when grain size is correlated with phase diagram variables and the bulk composition of the alloy is in the neighborhood of the solubility limit of a hypoeutectic alloy system. This is because the d vs P or Q curves are "U" shaped with their minimum in grain size occurring near the neighborhood of the solubility limit.

(4) The dependence of grain size on P or ΔT suggests that mechanisms associated with dendrite fragmentation and multiplication are the main operating mechanisms of grain refinement by solute elements in ingots and castings that are subjected to substantial convection during mold filling and subsequent solidification.

CRediT authorship contribution statement

Da-shan SUI: Investigation, data curation, Writing − Original draft, Writing − Review and editing; **Qing-you HAN:** Conceptualization, Methodology, Writing − Original draft, Writing − Review and editing, Supervision.

Declaration of competing interest

The authors declare that they have no known competing financial interests or personal relationships that could have appeared to influence the work reported in this paper.

Acknowledgments

This work was financially supported by the State Key Laboratory of Special Rare Metal Materials, China (No. SKL2021K002), and Northwest Rare Metal Materials Research Institute Ningxia Co., Ltd., China. The authors thank Dr. Shuang-lin CHEN from CompuTherm, LLC for providing the solidification range data of the alloys studied in this work.

Supplementary materials

Supplementary materials in this paper can be found at: http://tnmsc.csu.edu.cn/download/01-p1721-2022-

1327-Supplemental_materials.pdf.

References

[1] XIAO F, WU M, WANG Y X, ZHOU W Z, WANG S B, WANG D H, ZHU G L, JIANG M, SHU D, MI J W, SUN B D. Effect of trace boron on grain refinement of commercially pure aluminum by Al−5Ti−1B [J]. Transactions of Nonferrous Metals Society of China, 2022, 32: 1061−1069.

[2] MARTIN J H, YAHATA B D, HUNDLEY J M, MAYER J A, SCHAEDLER T A, POLLOCK T M. 3D printing of high-strength aluminium alloys [J]. Nature, 2017, 549: 365−369.

[3] COLLINS P C, BRICE D A, SAMIMI P, GHAMARIAN I, FRASER H L. Microstructural control of additively manufactured metallic materials [J]. Annual Review of Materials Research, 2016, 46: 63−91.

[4] HAN Q. A Model correlating fluidity to alloy variables in hypoeutectic alloys [J]. Acta Materialia, 2022, 226: 117587.

[5] HAN Q. Shrinkage porosity and gas porosity [M]//Ohio, USA: ASM International, 2008: 370−374.

[6] SCHUMACHER P, GREER A L. Heterogeneously nucleated α-Al in amorphous aluminium alloys [J]. Materials Science and Engineering A, 1994, 178: 309−313.

[7] MAXWELL I, HELLAWELL A. A simple model for grain refinement during solidification [J]. Acta Metallurgica, 1975, 23: 229−237.

[8] EASTON M A, STJOHN D H. A model of grain refinement incorporating alloy constitution and potency of heterogeneous nucleant particles [J]. Acta Materialia, 2001, 49: 1867−1878.

[9] YUAN L L, GUO M X, YAN Y, FENG W J, LIU Z Y, ZHUANG L Z. Theoretical design and distribution control of precipitates and solute elements in Al−Zn−Mg−Cu alloys with heterostructure [J]. Transactions of Nonferrous Metals Society of China, 2021, 31: 3328−3341.

[10] WEI Q, LU Z, YAO Q R, DENG J Q, WANG J, ZHOU H Y, RAO G H. Vertical section phase diagrams of La−Fe−B ternary system [J]. Transactions of Nonferrous Metals Society of China, 2021, 31: 1748−1757.

[11] HAN Q Y. The role of solutes in grain refinement of hypoeutectic magnesium and aluminum alloys [J]. Journal of Magnesium and Alloys, 2022, 10: 1846−1856.

[12] HAN Q Y. Revisiting the role of solutes in grain refinement of hypoeutectic alloys [J]. Metallurgical and Materials Transactions A, 2021, 52: 4234−4245.

[13] STJOHN D H, EASTON M A, QIAN M, TAYLOR J A. Grain refinement of magnesium alloys: A review of recent research, theoretical developments, and their application [J]. Metallurgical and Materials Transactions A, 2013, 44: 2935−2949.

[14] GREER A L, BUNN A M, TRONCHE A, EVANS P V, BRISTOW D J. Modelling of inoculation of metallic melts: Application to grain refinement of aluminium by Al−Ti−B [J]. Acta Materialia, 2000, 48: 2823−2835.

[15] JOHNSSON M, BACKERUD L. The influence of composition on Equiaxed crystal growth mechanisms and grain size in Al alloys [J]. International Journal of Materials Research, 1996, 87: 216−220.

[16] LIOTTI E, ARTETA C, ZISSERMAN A, LUI A, LEMPITSKY V, GRANT P S. Crystal nucleation in metallic alloys using X-ray radiography and machine learning [J]. Science Advances, 2018, 4(4): 1−9.

[17] EASTON M A, STJOHN D H, PRASAD A. Grain refinement of aluminium alloys: Recent developments in predicting the as-cast grain size of alloys refined by Al−Ti−B master alloys [J]. The Minerals, Metals & Materials Society, 2014, 20: 939−944.

[18] HAN L, VIAN C, SONG J, LIU Z, HAN Q, XU C, SHAO L. Grain refining of pure aluminum [J]. Light Metals, 2012: 967−971.

[19] ABDEL-REIHIM M, HESS N, REIF W, BIRCH M E J. Effect of solute content on the grain refinement of binary alloys [J]. Journal of Materials Science, 1987, 22: 213−218.

[20] XU H, XU L D, ZHANG S J, HAN Q. Effect of the alloy composition on the grain refinement of aluminum alloys [J]. Scripta Materialia, 2006, 54: 2191−2196.

[21] BIROL Y. Effect of solute Si and Cu on grain size of aluminium alloys [J]. International Journal of Cast Metals Research, 2013, 26(1): 22−27.

[22] TARSHIS L A, WALKER J L, RUTTER J W. Experiments on the solidification structure of alloy castings [J]. Metallurgical Transactions, 1971, 2: 2589−2597.

[23] SPITTLE J A, SADLI S. Effect of alloy variables on grain refinement of binary aluminum alloys with Al−Ti−B [J]. Materials Science and Technology, 1995, 11: 533−537.

[24] SMITH V G, TILLER W A, RUTTER J W. A mathematical analysis of solute redistribution during solidification [J]. Canadian Journal of Physics, 1955, 33: 723−745.

[25] NEUMANN-HEYME H, SHEVCHENKO N, LEI Z, ECKERT K, KEPLINGER O, GRENZER J, BECKERMANN C, ECKERT S. Coarsening evolution of dendritic sidearms: From synchrotron experiments to quantitative modeling [J]. Acta Materialia, 2018, 146: 176−186.

[26] ESKIN D G, ZUIDEMA J, SAVRAN V I, KATGERMAN L. Structure formation and macrosegregation under different process conditions during DC casting [J]. Materials Science and Engineering A, 2004, 384: 232−244.

[27] HAN Q, ZHANG J. Fluidity of alloys under high-pressure die casting conditions: flow-choking mechanisms [J]. Metallurgical and Materials Transactions B, 2020, 51: 1795−1804.

[28] HAN Q, HELLAWELL A. Primary particle melting rates and equiaxed grain nucleation [J]. Metallurgical and Materials Transactions B, 1997, 28(1): 169−173.

[29] VIAN C, KIBBEY C, CHEN Y, KUNTZ C, HAN Q. Cooling-assisted ultrasonic grain refining of aluminum E380 die casting alloy [J]. International Journal of Metalcasting, 2022, 16(2): 842−852.

[30] CHALMERS B. The structure of ingots [J]. Journal of the Australian Institute of Metals, 1963, 8: 255−263.

[31] ZIMMERMANN G, PICKMANN C, HAMACHER M, SCHABERGER-ZIMMERMANN E, NEUMANN-HEYME H, ECKERT K, ECKERT S. Fragmentation-driven grain refinement in directional solidification of AlCu10wt.% alloy at low pulling speeds [J]. Acta Materialia, 2017, 126:

236−250.
[32] HAN Q. Dendritic features of the solidification structure in a large AA3004 direct chill (DC) cast ingot [J]. Metallurgical and Materials Transactions B, 2022, 53: 786−797.
[33] FAN Z. Semisolid metal processing [J]. International Materials Reviews, 2002, 47: 49−85.
[34] HAN Q Y. Ultrasonic processing of materials [J]. Metallurgical and Materials Transactions B, 2015, 46: 1603−1614.
[35] HAN Q Y. Motion of bubbles in the mushy zone [J]. Scripta Materialia, 2006, 55: 871−874.
[36] VREEMAN C J, INCROPERA F P. The effect of free-floating dendrites and convection on macrosegregation in direct chill cast aluminum alloys (Part II): Predictions for Al−Cu and Al−Mg alloys [J]. International Journal of Heat and Mass Transfer, 2000, 43: 687−704.
[37] NADELLA R, ESKIN D G, KATGERMAN L. Role of grain refining in macrosegregation upon direct chill casting of AA2024 round billet [J]. Materials Science Forum, 2006, 519/520/521: 1841−1846.

亚共晶合金晶粒尺寸与相图变量相关双参数模型的检验

隋大山[1]，Qing-you HAN[2,3]

1. 上海交通大学 材料科学与工程学院 塑性成形与装备研究院，上海 200030；
2. 东南大学 机械工程学院，南京 211189；
3. School of Engineering Technology, Purdue University, West Lafayette, IN 47906, USA

摘 要：提出用于描述晶粒尺寸与工艺条件和相图变量相关联的简单双参数数学模型，然而，这些模型还没有通过良好的实验数据进行充分检验。采用精选的亚共晶合金实验数据检验这些模型，并提出实验数据的选择标准。采用这些双参数模型拟合被选择的实验数据，检查曲线的拟合质量和适用性，从而确定与实验数据吻合更好的数学模型。基于数据分析，探讨溶质元素细化晶粒尺寸的机理。结果表明，晶粒尺寸与合金凝固间隔之间存在明确的依赖关系，这种关系可采用 P 变量加以描述。晶粒尺寸对凝固间隔的这种明显依赖表明，在充型和凝固过程存在对流的铸锭和铸件中，与枝晶破碎有关的机理是控制溶质元素细化晶粒的主要运行机制。

关键词：凝固组织；晶粒细化；溶质元素；数学模型；相图变量；晶粒尺寸；亚共晶合金

(Edited by Xiang-qun LI)